2026 IEEE International Conference on Robotics and Automation (ICRA 2026)
June 1-5, 2026. Vienna, Austria

Comparative Analysis of Energy Transfers and Performance in Safety-Critical Control using Control Barrier Functions

Arturo Maiani*, Federico Califano†, Lorenzo Govoni* and Antonio Pietrabissa*

***Abstract*— Control barrier functions (CBFs) are used in safety-critical control strategies, implementing a modification of a nominal control action to achieve invariance of a subset of the state space representing safe operating conditions. In this paper we perform a comparative study involving existing safety-critical CBF designs, including energy-based CBFs and Exponential CBFs. The analysis, performed both theoretically and on a benchmark obstacle avoidance task, provides insights into how these CBFs affect energy transfers and the overall performance of the closed-loop system, highlighting benefits and limitations of each approach. To validate our analysis, we conduct software simulations on a 3R planar robot and a 7-DoF robotic manipulator, complemented by experimental evaluations on a physical robotic platform.**

***Index Terms*— Control barrier functions, Energy-based control, Nonlinear control, safety-critical control**

I. Introduction

Robotic applications rely on a nominal controller, typically designed to satisfy performance and stability requirements. In practice, performance objectives must be paired with safety specifications, often representing static or dynamic obstacles to be avoided during task execution [1], [2], [3]. This view of safety-critical control applications has led to the concept of *safety filters* [2], computational units that transform a nominal control input into one that i) minimally modifies the controller and ii) ensures safety. A popular technique for implementing safety filters is *control barrier functions* (CBFs) [1], [4], an algorithm which aims to modify a nominal control input to achieve forward invariance of a safe set. In some particular scenarios, safety specifications may conflict with the main task to be executed, leading to deterioration of performance, previously guaranteed by the nominal controller.

CBFs have been proposed for generic systems [5], [6] and robotics [7], [8], often managing positional constraints and generalizing Artificial Potential Fields [9]. Their use cases are diverse, including ensuring joint limits [6] and collision avoidance in multi-agent [10]. Recent research merges CBFs with energy-based techniques to guarantee safety and closed-loop passivity, including port-Hamiltonian frameworks [11], energy tanks [12], [13], time-varying CBFs [14], and optimization-based controllers [15]. This includes foundational work on passivity-preserving CBFs [16], with extensions to switched systems [17] and human-robot interaction [18].

This paper presents a systematic comparative study of two principal classes of CBFs for torque-controlled robotic manipulators: Energy-Based CBFs (EB-CBFs) [7], [8] and Exponential CBFs (ECBFs) [6]. The former is tailored to mechanical systems, enabling safety filter design without knowledge of Coriolis and centrifugal terms, while the latter is a general-purpose solution for control-affine systems that requires full model knowledge.

First, we generalize the result of [16] by proving that the EB-CBF from [8] preserves closed-loop passivity. Second, we empirically analyze how these CBFs affect performance and energy transfer in a benchmark obstacle avoidance task. The results reveal a critical trade-off, showing that despite their formal passivity guarantees, EB-CBFs can induce significant task performance degradation compared to ECBFs.

The remainder of the paper is organized as follows. In Sec. II, the background on robotic manipulator dynamic models and CBFs is reviewed. Sec. III describes the main contribution of this paper, i.e., the development of the energetic analysis of each CBF. In Sec. IV, numerical simulations are performed on a 3R planar robot to evaluate the proposed approach in a simplified setting. Sec. V extends this analysis to a more complex scenario, presenting both simulation results and real-world experiments on the 7-DoF KUKA LWR manipulator. Finally, in Sec. VI conclusions are drawn together with future works.

Notation. The set $\mathcal{C}^1$ refers to the set of continuously differentiable functions whose first derivative is continuous. Given a general dynamical system, the set $\mathcal{D}$ and the set $\mathcal{U}$ refer to the *state space* and *input space*, respectively. The expression $E(q, \dot{q})$ represents the total mechanical energy of a system. The function $\mathbb{1}_X(x) = \begin{cases} 1 & \text{if } x \in X \\ 0 & \text{if } x \notin X \end{cases}$ denotes the indicator function.

II. Background

We refer to [1], [4], [19], [7] regarding CBF for references that fully cover the presented background and to [20], [21] for preliminaries on modeling and control of robotic manipulators.

A. Control Barrier Functions

Consider the input-affine nonlinear system:

$$\dot{x} = f(x) + g(x)u, \tag{1}$$

*Arturo Maiani, Lorenzo Govoni and Antonio Pietrabissa are with the Department of Computer, Control and Management Engineering "Antonio Ruberti", Sapienza University of Rome (emails: {maiani, govoni, pietrabissa}@diag.uniroma1.it).

†Federico Califano is with the Robotics and Mechatronics (RaM) Department, University of Twente, The Netherlands (email: f.califano@utwente.nl).

where $x \in \mathcal{D} \subseteq \mathbb{R}^n$, $u \in \mathcal{U} \subseteq \mathbb{R}^m$, and f and g are continuously differentiable. A Lipschitz continuous controller ensures existence and uniqueness of solutions.

Definition 1. *The relative degree r of a differentiable function $b : \mathbb{R}^n \to \mathbb{R}$ with respect to* (1) *is the number of times it must be differentiated along the system dynamics until u explicitly appears.*

Control barrier functions represent a technique to guarantee forward invariance of a set $\mathcal{C}$, normally called *safe set*: the control goal is to design a state feedback $u(x) = k(x)$ for system (1) resulting in the closed-loop system $\dot{x} = f_{cl}(x) = f(x) + g(x)k(x)$ such that

$$\forall\ x(0) \in \mathcal{C} \implies x(t) \in \mathcal{C}\ \forall t > 0. \tag{2}$$

The safe set $\mathcal{C}$ is defined according to the class of CBF, which can be either *Zeroing* or *Reciprocal*:

1) Zeroing CBFs (Z-CBF): The safe set $\mathcal{C}$ is built as the superlevel set of a continuously differentiable function $h : \mathcal{D} \to \mathbb{R}$, i.e.,

$$\mathcal{C} = \{x \in \mathcal{D} : h(x) \geq 0\}. \tag{3}$$

The function $h(x)$ is then a *control barrier function* (CBF) on $\mathcal{D}$ if $\frac{\partial h}{\partial x}(x) \neq 0,\ \forall x \in \partial\mathcal{C}$ and

$$\sup_{u \in \mathcal{U}} [L_f h(x) + L_g h(x) u] \geq -\alpha(h(x)) \tag{4}$$

where $L_f h(x) = \frac{\partial h}{\partial x} f(x) \in \mathbb{R}, L_g h(x) = \frac{\partial h}{\partial x} g(x) \in \mathbb{R}^{1\times m}$, for all $x \in \mathcal{D}$ and some *extended class $\mathcal{K}$ function* α [1].

The following key result connects the existence of such CBF to forward invariance of the corresponding safe set.

Lemma 1. *[1]: Let $h(x)$ be a CBF on $\mathcal{D}$ for (1). Any locally Lipschitz controller $u(x) = k(x)$ such that $L_f h(x) + L_g h(x) k(x) \geq -\alpha(h(x))$ provides forward invariance of the safe set $\mathcal{C}$. Additionally, the set $\mathcal{C}$ is asymptotically stable on $\mathcal{D}$.*

The way controller synthesis induced by CBFs are implemented is to use them as *safety filters*, transforming a nominal state-feedback control input $u_{\text{nom}}(x)$ into a new state-feedback control input $u^*(x)$ in a minimally invasive fashion in order to guarantee forward invariance of $\mathcal{C}$. In practice, the following Quadratic Program (QP) is solved:

$$\begin{aligned} u^*(x) = &\arg\min_{u \in \mathcal{U}} \|u - u_{\text{nom}}(x)\|^2 \\ \text{s.t.} \quad &L_f h(x) + L_g h(x) u \geq -\alpha(h(x)). \end{aligned} \tag{5}$$

The transformation of the nominal control input $u_{\text{nom}}(x)$ in $u^*(x)$ by solving (5) is denoted as safety-critical control, or safety-critical filtering. Finally, the closed form solution to (5) is presented in the following lemma.

Lemma 2. *[4]: Let $h(x)$ be a Z-CBF on a set $\mathcal{D}$ for system (1), and assume $\mathcal{U} = \mathbb{R}^n$ and $L_g h(x) \neq 0,\ \forall x \in \mathcal{D}$. Define $\Psi_Z(x; u) = L_f h(x) + L_g h(x) u + \alpha(h(x))$, where $\alpha(\cdot)$ is a class $\mathcal{K}$-function, and $E_Z = \{x \in \mathcal{D}, u \in \mathcal{U} \mid \Psi_Z(x; u) < 0\}$, representing the set where the safety-critical filtering is applied. A closed-form solution for* (5) *is given by $u^*(x) = u_{\text{nom}}(x) + u_{\text{safe}}(x)$, where*

$$u_{\text{safe}}(x) = -\mathbb{1}_{E_Z}(x, u_{\text{nom}}) \frac{L_g h(x)^\top}{\|L_g h(x)\|^2} \Psi_Z(x; u_{\text{nom}}) \tag{6}$$

2) Reciprocal CBFs (R-CBFs): Reciprocal Control Barrier Functions (R-CBFs) were introduced in [22] and are characterized by the fact that they become unbounded at the boundary of the safe set $\mathcal{C}$, hence the term "barrier." Their formal definition is provided as follows.

Given a continuously differentiable function $h : \mathcal{D} \to \mathbb{R}$, define its superlevel set as $\mathcal{C} \subseteq \mathcal{D}$. The function $B : \text{Int}(\mathcal{C}) \to \mathbb{R}$ is referred to as an R-CBF defined for the set $\mathcal{C}$ if it satisfies the following conditions for all $x \in \text{Int}(\mathcal{C})$, namely:

$$\frac{1}{\alpha_1(h(x))} \leq B(x) \leq \frac{1}{\alpha_2(h(x))} \tag{7}$$

$$\inf_{u \in \mathbb{R}^n} [L_f B(x) + L_g B(x) u] < \alpha_3(h(x)), \tag{8}$$

$$L_g B(x) = 0 \quad \implies \quad L_f B(x) < \alpha_3(h(x)) \tag{9}$$

where α_1, α_2, and α_3 are *class-$\mathcal{K}$* functions [23]. If the R-CBF in (7)-(9) exists, forward invariance of set $\mathcal{C}$ is guaranteed, as stated in the following theorem.

Theorem 1. *[22]: Given a set $\mathcal{C} \subset \mathcal{D}$, defined as the superlevel set of a continuously differentiable function $h : \mathcal{D} \to \mathbb{R}$ as in* (3)*, if there exists a barrier function $B(x)$* (7)-(9)*, then $\mathcal{C}$ is forward invariant.*

Similarly to (5), the nominal state-feedback control input $u_{\text{nom}}(x)$ is filtered in a minimally invasive fashion in order to guarantee forward invariance of $\mathcal{C}$. The optimal control action $u^*(x)$ is found solving the following QP [24]:

$$\begin{aligned} u^*(x) = &\arg\min_{u \in \mathcal{U}} \|u - u_{\text{nom}}(x)\|^2 \\ \text{s.t.} \quad &L_f B(x) + L_g B(x) u \leq \alpha_3(h(x)) \end{aligned} \tag{10}$$

where $\mathcal{U} = \mathbb{R}^m$. The closed form solution of (10) is defined in the following lemma, similarly to the Z-CBF case.

Lemma 3. *[22]: Let $B(x)$ be a R-CBF on $\mathcal{D}$ for (1) and assume $\mathcal{U} = \mathbb{R}^m$ and $L_g B(x) \neq 0,\ \forall x \in \mathcal{D}$. Define $\Psi_R(x; u) = L_f B(x) + L_g B(x) u - \alpha_3(h(x))$. A closed-form solution for (6) is given by $u^*(x) = u_{\text{nom}}(x) + u_{\text{safe}}(x)$, where*

$$u_{\text{safe}}(x) = -\mathbb{1}_{E_R}(x, u_{\text{nom}}) \frac{L_g h(x)^\top}{\|L_g h(x)\|^2} \Psi_R(x; u_{\text{nom}}) \tag{11}$$

and $E_R = \{x \in \mathcal{D}, u \in \mathcal{U} \mid \Psi_R(x; u) > 0\}$ represents the set where the safety-critical filtering is applied.

For simplicity, we denote $\mathbb{1}_{E_Z}(x, u_{\text{nom}})$ and $\mathbb{1}_{E_R}(x, u_{\text{nom}})$ as $\mathbb{1}_{E_Z}$ and $\mathbb{1}_{E_R}$. Although both CBFs serve similar purposes, their structures differ: Z-CBFs are defined on the entire domain $\mathcal{D}$, whereas R-CBFs are restricted to the safe set $\mathcal{C}$, where the barrier diverges at the boundary. Consequently, Z-CBFs remain well-defined even outside $\mathcal{C}$, ensuring not only invariance but also attractivity of the safe set (Theorem 1). Their similarities and differences under a common application will be discussed through the proposed energy-based analysis.

[1] A function $\alpha : (-b, a) \to (-\infty, \infty)$ with $a, b > 0$, which is continuous, strictly increasing, and $\alpha(0) = 0$.

Having introduced the general theory of CBFs, we next turn to the case of robotic manipulators. Their mechanical structure can be framed into the input-affine formulation in (1) and allows for an energy-based analysis of the safety-critical actions induced by CBFs.

B. Model of a Fully Actuated Robot Manipulator

A common instance of (1) is a serial, fully actuated n-DoF robot manipulator with configuration $q \in Q$ and velocity $\dot{q} \in T_qQ$, where T_qQ is the tangent space at q, containing all possible velocity vectors. Its dynamics are described by

$$M(q)\ddot{q} + C(q,\dot{q})\dot{q} + G(q) = u, \tag{12}$$

where $M(q)$ is the inertia matrix, $C(q,\dot{q})$ captures Coriolis/centrifugal forces, $G(q)$ is gravity, and u is the actuation.

Defining the state $x = (q^\top, \dot{q}^\top)^\top \in TQ$, where TQ is the tangent bundle of Q (12) can be written in affine form (1) with $x \in \mathbb{R}^{2n}$. Analysis in this work is performed on these local coordinates. System (12) possesses properties central to our analysis, stated next.

Property 1. *The inertia matrix $M(q)$ is symmetric, positive definite, and bounded for any $q \in \mathbb{R}^n$.*

Property 2. *If the matrix $C(q,\dot{q})$ is defined through Christoffel symbols, then $\dot{M}(q) - 2C(q,\dot{q})$ is a skew symmetric matrix. This is equivalent to $\dot{M}(q) = C(q,\dot{q}) + C^\top(q,\dot{q})$.*

Property 3. *The time derivative of kinetic energy $K_e(q,\dot{q}) = \frac{1}{2}\dot{q}^\top M(q)\dot{q}$ along solutions of* (12) *is given by $\dot{K}_e(q,\dot{q}) = \dot{q}^\top[u - G(q)]$.*

C. Energy Based Analysis of CBFs on Mechanical Systems

In the domain of safety-critical control applied to mechanical systems, the expression for the power injected by the CBF control action u_{safe} in (6),(11) into system (12) can be analyzed by writing the power balance equation for mechanical energy. Consider the general expression of the mechanical energy $E(q,\dot{q}) = K_e(q,\dot{q}) + V(q)$, where $K_e(q,\dot{q})$ is the kinetic energy and $V(q)$ is the potential energy. Using property 3 and $\frac{\partial V}{\partial q} = G(q)$ it is easily seen that the power balance equation takes the following expression:

$$\dot{E} = \dot{K}_e + \dot{V} = \dot{q}^\top u_{\text{nom}} + \dot{q}^\top u_{\text{safe}} \tag{13}$$

The last term in the power balance corresponds to the power injected into system (12) by the safety-critical control, which can be further analyzed as follows.

Proposition 1. *Consider system* (12) *controlled with either a Z-CBF* (6) *or a R-CBF* (11)*. The power injection due to safety-critical control component $\dot{q}^\top u_{\text{safe}}$ results in*

$$P_{h,\alpha} := \dot{q}^\top u_{\text{safe}} = -\mathbb{1}_{E_i} \frac{\dot{q}^\top M^{-1}(q) \frac{\partial h}{\partial \dot{q}}^\top}{\| M^{-1}(q) \frac{\partial h}{\partial \dot{q}}^\top \|^2} \Psi_i. \tag{14}$$

where $i = Z, R$ in case of ZCBF and RCBF, respectively.

Proof: Consider the mechanical system (12) with state $x = (q^\top, \dot{q}^\top)^\top \in TQ$, rewritten in the input-affine state space model (1). The corresponding input vector field is defined as $g(q,\dot{q}) = [0_{n\times n}, M^{-1}(q)]^\top$. The expression for $P_{h,\alpha}$ is obtained substituting the Lie derivative $L_g h(q,\dot{q}) = \frac{\partial h}{\partial \dot{q}} M^{-1}(q)$ in the closed form expressions (6)-(11), yielding the result.

A special case is analyzed in the following lemma from [16], when the power injected in the system takes negative values.

Lemma 4. *[16]: Let system* (12) *controlled with a nominal control action $u = u_{\text{nom}}(q,\dot{q})$ result in a closed-loop system stable in the sense of Lyapunov with respect to a desired Lyapunov function $S_{cl}(q,\dot{q})$ of the form:*

$$S_{cl}(q,\dot{q}) = K_e(q,\dot{q}) + V_d(q), \tag{15}$$

where $V_d(q) \geq 0$ is a positive definite function of the configuration variables $q \in Q$. If the safety-filtering action induced by a CBF $h(q,\dot{q})$ is such that $P_{h,\alpha} < 0$, then $S_{cl}(q,\dot{q})$ is still a Lyapunov function for closed-loop system subject to the safety-filtering action.

In particular, we focus our attention on the class of mechanical systems controlled by a PD control law with gravity compensation of the form

$$u_{\text{nom}} = -D\dot{q} - Pe + G(q) \tag{16}$$

where $P \in \mathbb{R}^n$ and $D \in \mathbb{R}^n$ are positive definite matrices and $e := q - q_d$. The nominal control law (16) guarantees that the closed-loop energy function $S_{cl}(q,\dot{q})$ is a Lyapunov Function for system (12) with nominal equilibrium $(q_d^\top, 0^\top)^\top$ and $V_d(q) = \frac{1}{2}\|e\|_P^2$, $P > 0$. For this class of systems the energy balance takes the form:

$$\dot{S}_{cl} = -\dot{q}^\top D\dot{q} + P_{h,\alpha}. \tag{17}$$

Equation (17) can be obtained by substituting expression (16) and $\frac{\partial V_d}{\partial q} = e^\top P$ into the following energy balance equation and:

$$\dot{S}_{cl} = \dot{q}^\top[u_{\text{nom}} + u_{\text{safe}} - G(q)] + \frac{\partial V_d}{\partial q}\dot{q}. \tag{18}$$

In the following section, we further analyse the CBF from an energetic perspective, comparing the main classes of such control technique.

III. CBFs for safety-critical control of Robotic Manipulators

Applying control barrier functions to robotic manipulators poses challenges beyond the general affine case. In mechanical systems, safety constraints are often expressed as functions of configuration variables, $\phi(q) : Q \to \mathbb{R}$ with $Q \subseteq \mathbb{R}^n$, leading to a safe set of the form:

$$\mathcal{S} = \{q \in Q \mid \phi(q) \geq 0\}. \tag{19}$$

However, for second-order dynamics such as torque-controlled manipulators (12), a barrier function of the form (19) yields relative degree greater than one, i.e. $L_g\phi(q) = 0_{1\times n}$. As a result, the standard CBF formulation (5) cannot be applied directly, since the control input u does not appear in the constraint. To overcome this limitation, several works [9], [8], [6] propose defining barrier functions

$h(q,\dot{q}) : TQ \to \mathbb{R}$ that explicitly depend on both position and velocity, ensuring that $L_g h(q,\dot{q}) \neq 0$ when the safety condition becomes active.

We analyze these CBFs by examining the power injected into the nominal closed-loop system by the safety-critical action. The first two types [7], [8] fall under Stability Preserving CBFs [25], where $P_{h,\alpha} \leq 0$ guarantees stability. By contrast, CBFs such as [6] yield $P_{h,\alpha}$, indefinite in sign, providing no stability guarantee. In what follows, we discuss the resulting trade-offs between task performance and stability.

A. Energy Based Z-CBFs

An interesting type of Z-CBF which deserves some discussion is the one developed in [7], that works by subtracting the kinetic energy of the system to the function $\phi(q)$, scaled by a positive constant $\beta \in \mathbb{R}^+$:

$$h(q,\dot{q}) = \beta\phi(q) - K_e(q,\dot{q}). \tag{20}$$

The CBF (20) is such that its superlevel set $\bar{\mathcal{S}}$ can be expressed as

$$\bar{\mathcal{S}} = \{(q,\dot{q}) \in TQ \mid h(q,\dot{q}) \geq 0\}, \tag{21}$$

and is always contained in $\mathcal{S}$ (19), with $\lim_{\beta\to\infty} \bar{\mathcal{S}} = \mathcal{S}$. The safety-critical control action (6) takes the following expression:

$$u_{\text{safe}}(x) = \mathbb{1}_{E_Z} \frac{\dot{q}}{\|\dot{q}\|^2} \Psi_Z(q,\dot{q},u_{\text{nom}}). \tag{22}$$

Property 4. *[16] The sign of the instantaneous power injection* (14) *obtained by applying CBF* (20) *on system* (12) *is negative semi-definite:*

$$P_{h,\alpha} = \mathbb{1}_{E_Z} \Psi_Z(q,\dot{q},u_{\text{nom}}) \leq 0, \tag{23}$$

where $\Psi_Z(q,\dot{q},u_{\text{nom}})$ *takes the form:*

$$\Psi_Z(q,\dot{q},u_{\text{nom}}) = \dot{q}^\top \left[\beta \frac{\partial\phi}{\partial q}^\top + g(q) - u_{\text{nom}}\right] + \alpha(h(q,\dot{q})). \tag{24}$$

Note that due to the non-positive sign of the injected power (23), this CBF type preserves the stability of the overall system. The expression in (20) is a valid CBF since $\dot{q} = 0$ implies $\Psi_Z(q,\dot{q},u_{\text{nom}}) = \alpha(h(q,\dot{q})) > 0$, hence it does not activate the safety-critical constraint [7].

B. Energy Based R-CBF

In this section we calculate the power injected by safety-critical controller induced by the R-CBF presented in [8], defined as:

$$h(q,\dot{q}) = \frac{1}{\phi(q)} + \frac{K_e(q,\dot{q})}{1 + K_e(q,\dot{q})}. \tag{25}$$

We present a property for R-CBFs, analogous to Property 4 for Z-CBFs.

Property 5. *The sign of the instantaneous power injection* (14) *obtained by applying CBF* (25) *on system* (12) *is negative semi-definite:*

$$P_{h,\alpha} = -\mathbb{1}_{E_R} (1 + K_e)^2 \Psi_R \leq 0. \tag{26}$$

where $\Psi_R(q,\dot{q},u_{\text{nom}})$ *takes the form:*

$$\Psi_R(q,\dot{q},u_{\text{nom}}) = -\tfrac{L_f h(q,\dot{q})}{h(q)^2} + \tfrac{\dot{q}^\top (u_{\text{nom}} - G(q))}{(1+K_e(q,\dot{q}))^2} - \alpha(h(q,\dot{q})). \tag{27}$$

Proof: The result in (26) follows from the relation $\frac{\partial h}{\partial \dot{q}} = \frac{\dot{q}^\top M(q)}{(1+K_e)^2}$, which, when substituted into (14), yields the stated expression. Equation (27) is obtained by applying proposition (3) to $\dot{h}(q,\dot{q},u)$.

C. Exponential CBFs

Another approach to define Z-CBFs for safety-critical control of mechanical systems is represented by [26], which introduced the concept of a safety index, further investigated in [6] as Exponential CBFs, and generalized to time varying systems in [5] as Higher Order CBFs. In the domain of mechanical systems, a valid form for an Exponential CBF is:

$$h(q,\dot{q}) = \phi(q) + \gamma \frac{\partial\phi}{\partial q}\dot{q}, \tag{28}$$

with $\gamma \in \mathbb{R}_{>0}$. Thanks to the differentiability assumption $\phi \in \mathcal{C}^1$ and to the fact that the $\gamma \geq 0$, it holds that the safe set $\bar{\mathcal{C}} = \{q,\dot{q} \in TQ : h(q,\dot{q}) \geq 0\}$ defines a positively invariant set in $\mathcal{S}$ (19), i.e., $\bar{\mathcal{C}} \in \mathcal{S}$ [26]. Considering that $\frac{\partial h}{\partial \dot{q}} = \gamma \frac{\partial\phi}{\partial q}$, the power injected in the system (14) by the safety-critical filtering action (28) takes the following expression:

$$P_{h,\alpha} = -\mathbb{1}_{E_Z} \frac{\dot{q}^\top M^{-1}(q) \frac{\partial\phi}{\partial q}^\top}{\gamma \|M^{-1}(q) \frac{\partial\phi}{\partial q}^\top\|^2} \Psi_Z(q,\dot{q},u_{\text{nom}}) \tag{29}$$

where function Ψ_Z takes the form:

$$\Psi_Z = \alpha\phi(q) + (1+\gamma\alpha)\frac{\partial\phi}{\partial q}\dot{q} + \gamma\frac{\partial\phi}{\partial q}\ddot{q} + \gamma\dot{q}^\top \frac{\partial^2\phi}{\partial q^2}\dot{q}. \tag{30}$$

Note that the power expression in (29) is indefinite in sign and, in general, does not preserve stability. In particular, stability guarantees are lost if simultaneously $\Psi_Z < 0$ and $\dot{q}^\top M^{-1}(q) \frac{\partial\phi}{\partial q}^\top > 0$.

It must be noted that Exponential CBFs may lead to undesired performance as well. In particular, in the following lemma we prove that invariant sets different from the desired equilibrium can arise when using Exp-CBFs on system (12), nominally controlled with (16).

Lemma 5. *Consider system* (12) *under control law* (16) *with the CBF filter* (28). *Let* $Q_\phi = \{q \in Q : \phi(q) = 0\}$ *and define*

$$\Omega = \{q \in Q_\phi,\ \dot{q} = 0,\ \lambda \in \mathbb{R} \mid \Psi_Z < 0,\ Pe = \lambda M^{-1}(q) \frac{\partial\phi}{\partial q}^\top\}. \tag{31}$$

Then Ω *is invariant.*

Proof: For $\mathbb{1}_{E_Z} < 0$, the closed-loop dynamics are

$$M(q)\ddot{q} = C(q,\dot{q})\dot{q} + G(q) + u_{\text{nom}} + u_{\text{safe}}. \tag{32}$$

At $(q,\dot{q}) = (\tilde{q},0)$ with $\tilde{q} \in \Omega$, $u_{\text{nom}} = -G(q) - Pe$ and

$$u_{\text{safe}} = \mathbb{1}_{E_Z} \frac{M^{-1}(q) \frac{\partial\phi}{\partial q}^\top \frac{\partial\phi}{\partial q} M^{-1}(q)}{\|M^{-1}(q) \frac{\partial\phi}{\partial q}^\top\|^2} Pe.$$

Substituting into (32) gives

$$\|M^{-1}(q) \frac{\partial\phi}{\partial q}^\top\|^2 Pe = \left(M^{-1}(q) \frac{\partial\phi}{\partial q}^\top \frac{\partial\phi}{\partial q} M^{-1}(q)\right) Pe. \tag{33}$$

CBF Expression	Barrier-Type	Injected power	Stability Preserving	Related works	ID
$\beta\phi(q) - K_e(q,p)$	Z-CBF	$\mathbb{1}_{E_Z}\Psi(q,\dot{q},u_{\text{nom}})$	Yes	[7], [16], [25]	I
$\frac{1}{\phi(q)} + \frac{K_e(q,\dot{q})}{1+K_e(q,\dot{q})}$	R-CBF	$-\mathbb{1}_{E_R}(1+K_e)^2\Psi(q,\dot{q},u_{\text{nom}})$	Yes	[8]	II
$\phi(q) + \gamma\frac{\partial\phi}{\partial q}\dot{q}$	Z-CBF	$-\mathbb{1}_{E_Z}\frac{\dot{q}^\top M^{-1}(q)\frac{\partial\phi}{\partial q}^\top}{\gamma\|M^{-1}(q)\frac{\partial\phi}{\partial q}^\top\|^2}\Psi(q,\dot{q},u_{\text{nom}})$	No	[26],[27], [5],[6]	III

TABLE I: Comparison of CBF formulations, barrier type, injected power, and stability-preserving properties.

	Parameter	P	D	α	β	γ
Value	*Case A*	10	10	1	100	100
	Case B	10	10	1	30	1

TABLE II: Parameters for the nominal controller and the CBFs in software simulations on a 3R planar robot.

Since the matrix is symmetric rank-1, its only nonzero eigenvalue is $\lambda = \|M^{-1}(q)\frac{\partial\phi}{\partial q}^\top\|^2$ with eigenvector $v = M^{-1}(q)\frac{\partial\phi}{\partial q}^\top$. Hence the condition in (31) holds and Ω is invariant.

The previous theorem characterizes conditions under which stationary points may arise, namely when $\dot{q} = 0$ and $\phi(q) = 0$. In this case, the obstacle geometry may cause the proportional control term to balance the action of the safety filter. A full analysis of solutions to (31) is beyond the scope of this work, though such results could provide guarantees on the absence of undesired stationary points.

IV. Simulations: 3R planar robot

In this section a comparative analysis regarding performance and power transfer between different CBFs through simulations on a planar 3R robotic manipulator is performed. A nominal PD control law is designed to move the robot from its initial to a nominal joint configuration. A 2D virtual obstacle, depicted as a grey circle in the plots, is introduced along the robot's trajectory. To account for the obstacle, we define the function $\phi(q)$, used in all the CBF expressions, as follows

$$\phi(q) = [x_c - x_{EE}(q)]^2 + [y_c - y_{EE}(q)]^2 - r^2 \qquad (34)$$

where x_c and y_c are the obstacle center coordinates, r is the obstacle radius and $x_{EE}(q)$ and $y_{EE}(q)$ denote the coordinates of the robot manipulator end-effector. Moreover, the desired configuration is depicted in red in the plots.

Two scenarios, *Case A* and *Case B*, illustrate different system behaviors. In *Case A*, the desired joint configuration is $q_d = (\pi, -\pi/6, -\pi/3)^\top$, corresponding to a positive value for the third joint. Conversely, *Case B* is defined with $q_d = (\pi, -\pi/6, \pi/3)^\top$, where the third joint assumes a negative value. The parameter values for the nominal controller and the CBFs used in both cases are summarized in Table II. All software simulations are performed with a time discretization of $T_s = 10^{-5}s$ and the dynamics is integrated using Runge-Kutta-Fehlberg method.

The stability-preserving nature of energy-based CBFs (CBF-I and CBF-II), reported in Fig. 1d and Fig. 1e, yields high control effort during obstacle avoidance, as highlighted by the control peaks in Fig. 1c. On the other hand, the Exponential CBF allows for a larger reconfiguration to overcome the obstacle, as reported in Fig. 1f, thus avoiding excessive peaks in the control signal. Moreover, in Fig. 1a the CBF profile of the three approaches is reported, where a box highlights the time evolution of the first two seconds to show better that none of the CBF violates the safety requirement.

In Fig. 1g- 1l, the simulation results of *Case B* are reported, where the limitations of energy-based CBFs are visible. Specifically, both CBF-I and CBF-II fail to avoid the obstacle, see Fig. 1j and Fig. 1k respectively. The task requires a large reconfiguration that violates the stability-preserving condition—permissible under CBF-III, as demonstrated by the peak in the closed-loop energy in Fig. 1h. With large reconfigurations, energy-based CBFs perform poorly. Such CBFs can only dissipate power, therefore when the reconfiguration requires an increase of the value of potential function $V_d(q)$, the robot significantly slows down during the task execution. This effect is clearly visible in Fig. 1j and Fig. 1k where the robot halts in front of the obstacle, unable to complete the regulation task. When $\dot{q} \approx 0$, these CBFs exhibit chattering from numerical errors, as shown in Fig. 1i. Conversely, as demonstrated in *Case A*, CBF-III successfully avoids the obstacle and reaches the desired configuration as shown in Fig. 1l.

V. Simulations and Experiments: KUKA LWR IV+

The experimental setup uses a fully actuated KUKA LWR-IV+ at the Robotics Laboratory, Università di Roma "La Sapienza". This lightweight, seven-DoF anthropomorphic manipulator is equipped with encoders for joint positions and torque sensors on each joint. The robot is controlled via a KR-C2 unit with the Fast Research Interface (FRI) [28], which provides access to joint positions and torques.

A nominal joint reference q_d is generated by integrating the robot dynamics under the virtual control input u, derived from either CBF-I (20), CBF-II (25), or CBF-III (28). This reference is sent to the FRI, which applies the corresponding torques. Joint positions are measured directly, while velocities are obtained numerically from position data and filtered to reduce noise.

A. Simulation: single obstacle scenario

This section presents the simulation results for the KUKA LWR in addressing the collision avoidance through the CBF formalism. The simulation parameters for the nominal controller and the various CBFs are provided in Table III.

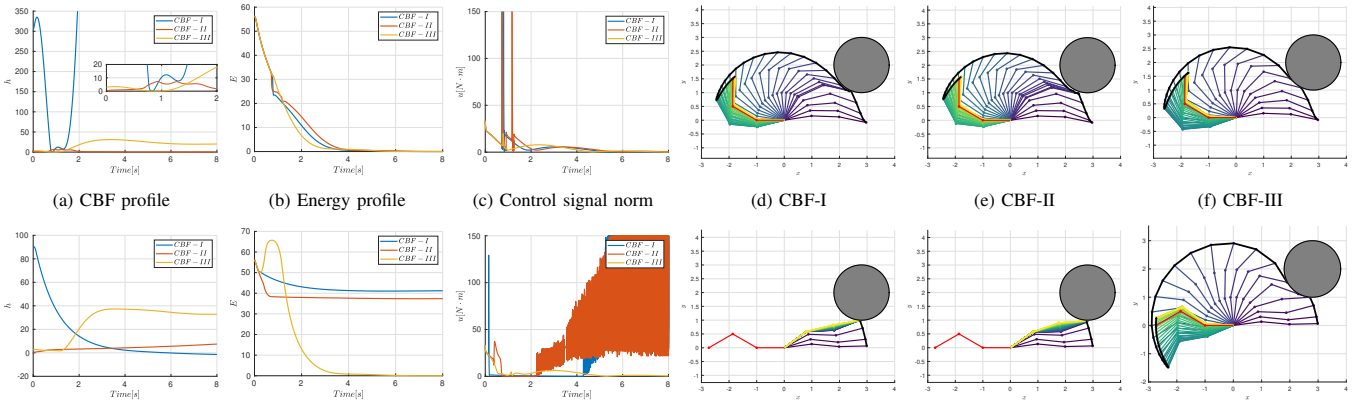

(a) CBF profile (b) Energy profile (c) Control signal norm (d) CBF-I (e) CBF-II (f) CBF-III

(g) CBF profile (h) Energy profile (i) Control signal norm (j) CBF-I (k) CBF-II (l) CBF-III

Fig. 1: 3R simulation results: *Case A* (top row) and *Case B* (bottom row).

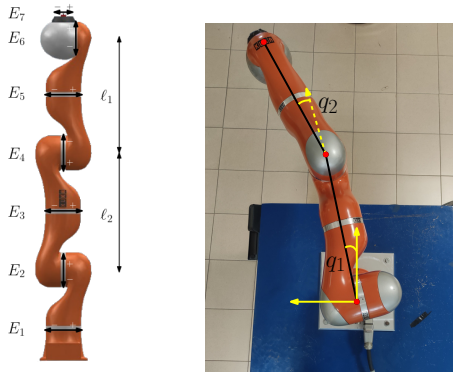

(a) KUKA LWR IV+ axes (b) 2R equivalent robot

Fig. 2: KUKA LWR IV+ Robot.

Parameter	P	D	α	β	γ
Value	10	10	10	100	9e-5

TABLE III: Simulation parameters for the nominal controller and the CBFs in the simulation on the KUKA LWR in the single obstacle scenario.

To evaluate collision avoidance capabilities, a virtual obstacle modeled as a 3D sphere is placed along the robot's trajectory. To account for the obstacle, the spatial formulation of the function $\phi(q)$, introduced in (34), is employed. The resulting expression is given by:

$$\phi(q) = [x_c - x_{EE}(q)]^2 + [y_c - y_{EE}(q)]^2 + [z_c - z_{EE}(q)]^2 - r^2, \quad (35)$$

where x_c, y_c, and z_c represent the coordinates of the obstacle center, r is the obstacle radius, and $x_{EE}(q)$, $y_{EE}(q)$, and $z_{EE}(q)$ denote the coordinates of the robot's end-effector as a function of the joint configuration q.

Fig. 3 illustrates a comparison of the different control strategies applied to the KUKA LWR IV+. As shown in Fig. 3f, CBF-III is the only safety-critical approach that successfully enables the robot to avoid the virtual obstacle. This is confirmed by the region highlighted in the box of Fig. 3a, where the safety function satisfies $h(q) > 0$ during the whole simulation. In contrast, CBF-I fails to ensure safety, resulting in a collision with the obstacle, represented by the CBF entering the region where $h(q) < 0$.

CBF-II, owing to its stability-preserving nature, is unable to compute a feasible control input that avoids the obstacle without violating the energy constraints of the closed-loop system. As a result, the robot comes to a halt in front of the obstacle, remaining on the boundary of the safe set, where $h(q) = 0$. Additionally, both CBF-I and CBF-II exhibit a chattering effect in the control signal, as depicted in Fig. 3c. This behavior arises from the challenging objectives of maintaining safety while preserving system stability.
Furthermore, it is important to note that the computational complexity of the control law derived using CBF-III may be higher compared to the other two approaches, primarily due to the evaluation of the terms $C(q, \dot{q})$ and $\frac{\partial^2 \phi}{\partial q^2}$. However, these expressions can be symbolically computed offline, enabling efficient numerical evaluation during real-time task execution, not compromising the execution speed of method-III relative to the other two approaches.

Fig. 3d- 3f provide a visual representation of the KUKA robot, including both its initial and desired configurations. In particular, Fig. 3f shows that, under CBF-III, the robot successfully avoids the obstacle by passing over it, an action that yields an increase in the system's closed-loop energy, shown in Fig. 3b.

B. Simulation: multiple obstacles scenario

This section considers the same simulation setup as before but with a harder collision-avoidance task. Two spherical obstacles of different sizes are placed along the KUKA trajectory, requiring simultaneous handling of multiple safety constraints. Following [29], a single CBF is built using Boolean logic to encode complex specifications. For each obstacle, a function ϕ_i (as in (35)) is defined from its center and radius, and the overall safe set $\mathcal{C}$ is obtained by combining $\mathcal{C}_1$ and $\mathcal{C}_2$ through a logical AND, implemented via the min operator:

$$\mathcal{C} = \mathcal{C}_1 \cap \mathcal{C}_2 = \{q \in \mathbb{R}^n : \min_{i=1,2} h_i(q) \geq 0\}. \quad (36)$$

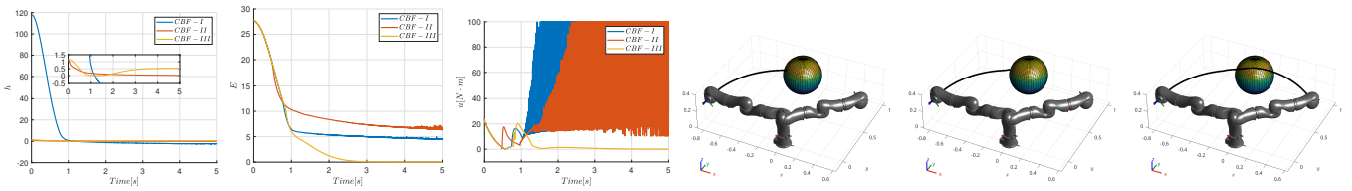

(a) CBF profile (b) Energy profile (c) Control signal norm (d) CBF-I (e) CBF-II (f) CBF-III

Fig. 3: KUKA 7-DoF simulation results: single obstacle scenario - performance metrics (left) and end-effector trajectories (right).

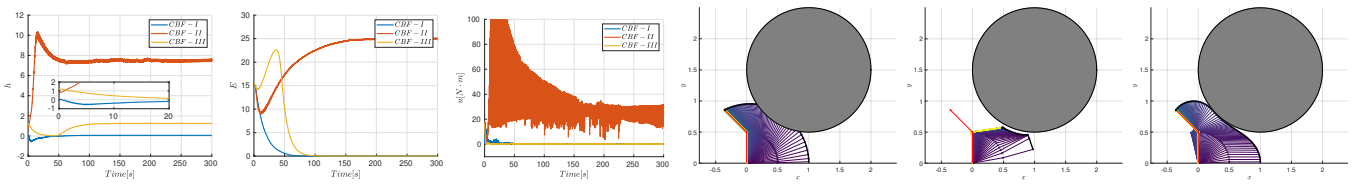

(a) CBF profile (b) Energy profile (c) Control signal norm (d) CBF-I (e) CBF-II (f) CBF-III

Fig. 4: KUKA experimental results: performance metrics (left) and end-effector trajectories (right).

Parameter	P	D	α	β	γ
Value	10	20	0.8	0.05	0.1

TABLE IV: Parameters for the nominal controller and the CBFs in the experiment.

However, the use of the min operator may lead to a function that is not continuously differentiable with respect to q, and therefore not a valid CBF. To address this, [29] proposes a smooth approximation of the min function, resulting in the following CBF formulation:

$$h(q) = -\frac{1}{\kappa} \ln \left(e^{-\kappa h_1(q)} + e^{-\kappa h_2(q)} \right), \tag{37}$$

where $\kappa > 0$ is a smoothing parameter. In our implementation, we choose $\kappa = 300$.

For clarity, Fig. 5 shows simulation results for CBF-III only, as it is the only method that successfully completes the obstacle-avoidance task in all cases. Figs. 5d–5e depict the robot trajectory around two obstacles of different sizes from different viewpoints. Note that the CBF in (37) accounts only for the end-effector position, not the volume of the last link. Fig. 5a shows the CBF profile, confirming $h(q) > 0$ throughout the entire simulation and demonstrating effective obstacle avoidance while reaching the desired configuration.

C. Experimental setup

To provide further insight into the behavior of the proposed control strategies, this section presents an experimental scenario based on the KUKA LWR IV+. While the previous sections employed the full 7-DoF KUKA LWR, here the analysis focuses on an equivalent 2R planar robot that preserves the essential features of the collision avoidance task while simplifying the dynamics.

The axes E_i $(i = 2, 3, 5, 6, 7)$ in Fig. 2a remain fixed, simplifying the KUKA robot to a 2R planar model (Fig. 2b). The controller and CBF parameters are given in Table IV.

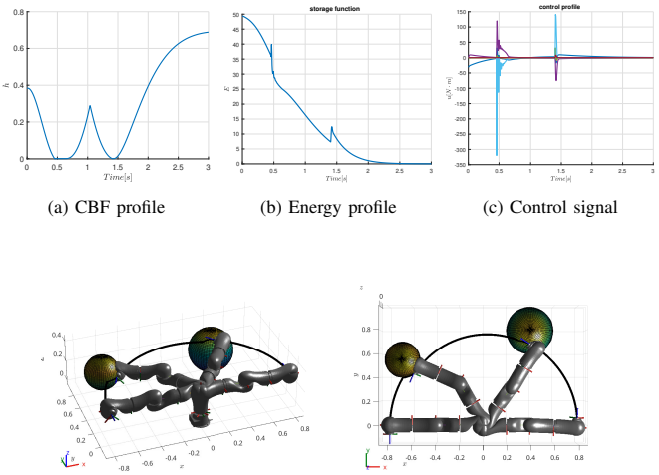

(a) CBF profile (b) Energy profile (c) Control signal

(d) Trajectory: side view (e) Trajectory: top view

Fig. 5: KUKA simulation plots: multiple obstacle scenario.

Fig. 4 presents the comparative analysis of the experimental results on the KUKA LWR IV+, when the different CBF approaches are used. Consistent with the simulations on the 3R planar robot in Section IV and on the KUKA LWR in Section V, due to chattering effects, the CBF-I method fails to ensure safety, resulting in $h(q) < 0$ during the time window when the robot *virtually* collides with the obstacle, as reported in Fig. 4a. Furthermore, a zoom on the first 20 seconds of simulation is reported to show that all the CBF profiles are positive at $t = 0$, as the robot starts in a safe configuration. Although CBF-II is theoretically proven to preserve stability, as shown in (26), the closed-loop energy profile increases while avoiding the obstacle, see Fig. 4b. This increase is due to the robot ending in a state where $\dot{q} \approx 0$, resulting in an undesirable chattering behavior in the control action leading to an increase in the potential function $V_d(q)$, as shown in *Case B* of the 3R simulation.

Moreover, similarly to software simulation results, CBF-III is the only technique that successfully achieves safety in avoiding the obstacle, while guiding the robot to its desired configuration. The fact that CBF-III is not stability preserving, allows the robot to fold in a configuration with negative q_2 values to avoid the obstacle, as highlighted by the increase in the total closed-loop energy in Fig. 4b. In conclusion, Fig. 4 shows results consistent with those in Fig. 3 and with *Case B* in Fig. 1. The robot controlled with CBF-I violates the safety constraint by entering the virtual obstacle (see Fig. 4d), while CBF-II causes the robot to stall in front of the obstacle (see Fig. 4e), again due to the inability to increase the closed-loop energy to perform the necessary motion. CBF-III, on the other hand, successfully guides the robot around the obstacle, as shown in Fig. 4f.

VI. Conclusions

This paper presented a comparative study of Energy-Based and Exponential Control Barrier Function (CBF) designs. Theoretical analysis and practical evaluation in an obstacle avoidance task provided insights into their effect on energy transfer and system performance. The analysis was validated through software simulations on 3R and 6-DoF robotic manipulators, and experiments on a physical 2R robot, confirming the theoretical predictions and real-world applicability of the different CBF designs. Future work will analyze energy-injecting CBFs for achieving desired closed-loop behavior [25] and extend the analysis to time-varying obstacle avoidance [30].

References

[1] A. Ames, S. Coogan, G. Notomista, P. Fernandes, and P. Tabuada, "Control barrier functions: Theory and applications," in *2019 18th European Control Conference (ECC)*. IEEE, 2019, pp. 3420–3431.

[2] K. Waber, A. Ames, and P. Tabuada, "Data-driven safety filters: Hamilton-jacobi reachability, control barrier functions, and predictive methods for uncertain systems," *IEEE Control Systems*, vol. 43, no. 5, pp. 137–177, 2023.

[3] F. Ferraguti, A. Villa, A. De Luca, and G. Ferretti, "Safety and efficiency in robotics: The control barrier functions approach," *IEEE Robotics and Automation Magazine*, vol. 29, no. 3, pp. 139–151, 2020.

[4] A. Ames, X. Xu, J. Grizzle, and P. Tabuada, "Control barrier function based quadratic programs for safety critical systems," *IEEE Transactions on Automatic Control*, vol. 62, no. 8, pp. 3861–3876, 2017.

[5] W. Xiao and C. Belta, "High-order control barrier functions," *IEEE Transactions on Automatic Control*, vol. 67, no. 7, pp. 3655–3662, 2022.

[6] Q. Nguyen and K. Sreenath, "Exponential control barrier functions for enforcing high relative-degree safety-critical constraints," in *2016 American Control Conference (ACC)*, 2016, pp. 322–328.

[7] A. Singletary, S. Kolathaya, and A. Ames, "Safety-critical kinematic control of robotic systems," in *Proceedings of the American Control Conference*, vol. 2021-May. IEEE, 2021, pp. 14–19.

[8] S. Kolathaya, "Energy based control barrier functions for robotic systems," Aug. 2020, techRxiv.

[9] A. Singletary, K. Klingebiel, J. Bourne, A. Browning, P. Tokumaru, and A. Ames, "Comparative analysis of control barrier functions and artificial potential fields for obstacle avoidance," in *2021 IEEE/RSJ International Conference on Intelligent Robots and Systems (IROS)*. IEEE, 2021, pp. 8129–8136.

[10] X. Tan and D. V. Dimarogonas, "Distributed implementation of control barrier functions for multi-agent systems," *IEEE Control Systems Letters*, vol. 6, pp. 1879–1884, 2021.

[11] M. Z. Romdlony and B. Jayawardhana, "Stabilization with guaranteed safety using control lyapunov–barrier function," *Automatica*, vol. 66, pp. 39–47, 2016.

[12] B. Capelli, C. Secchi, and L. Sabattini, "Passivity and control barrier functions: Optimizing the use of energy," *IEEE Robotics and Automation Letters*, vol. 7, no. 2, pp. 1356–1363, 2022.

[13] R. Califano, F. Rashad, C. Secchi, and S. Stramigioli, "The use of energy tanks for robotics systems," in *Soft Robotics*. Springer, 2018, pp. 172–188.

[14] G. Notomista, X. Cai, J. Yamauchi, and M. Egerstedt, "Passivity-based decentralized control of multi-robot systems with delays using control barrier functions," in *2019 International Symposium on Multi-Robot and Multi-Agent Systems (MRS)*, 2019, pp. 231–237.

[15] H. M. Sweatland, A. Isaly, E. J. Griffis, and W. E. Dixon, "Optimization-based controllers for passivity and safety constraints," *IEEE Transactions on Automatic Control*, pp. 1–8, 2024.

[16] F. Califano, "Passivity-preserving safety-critical control using control barrier functions," *IEEE Control Systems Letters*, vol. 7, pp. 1742–1747, 2023.

[17] Q. Meng, A. Kasis, and M. M. Polycarpou, "Passivity preserving safety-critical control of switched systems," in *2024 IEEE 63rd Conference on Decision and Control (CDC)*, 2024, pp. 8596–8601.

[18] W. S. Cortez, C. K. Verginis, and D. V. Dimarogonas, "Safe, passive control for mechanical systems with application to physical human-robot interactions," in *2021 IEEE International Conference on Robotics and Automation (ICRA)*, 2021, pp. 3836–3842.

[19] X. Xu, P. Tabuada, J. Grizzle, and A. Ames, "Robustness of control barrier functions for safety critical control," in *IFAC-PapersOnLine*, vol. 48, no. 27. IFAC, 2015, pp. 54–61.

[20] B. Siciliano, L. Sciavicco, L. Villani, and G. Oriolo, *Robotics: Modelling, Planning and Control*. Springer Publishing Company, Incorporated, 2010.

[21] M. W. Spong, S. A. Hutchinson, and M. Vidyasagar, "Robot modeling and control," *IEEE Control Systems*, vol. 26, no. 6, pp. 113–115, 2006.

[22] A. D. Ames, J. W. Grizzle, and P. Tabuada, "Control barrier function based quadratic programs with application to adaptive cruise control," in *53rd IEEE Conference on Decision and Control*, 2014, pp. 6271–6278.

[23] M. Jankovic, "Robust control barrier functions for constrained stabilization of nonlinear systems," *Automatica*, vol. 96, pp. 359–367, 2018.

[24] R. A. Freeman and P. V. Kokotovic, *Robust nonlinear control design: state-space and Lyapunov techniques*. USA: Birkhauser Boston Inc., 1996.

[25] F. Califano, R. Zanella, A. Macchelli, and S. Stramigioli, "The effect of control barrier functions on energy transfers in controlled physical systems," 2024.

[26] C. Liu and M. Tomizuka, "Control in a safe set: Addressing safety in human-robot interactions," in *ASME 2014 Dynamic Systems and Control Conference, DSCC 2014*, vol. 3, 11 2014.

[27] S. Liu, C. Liu, and J. M. Dolan, "Safe control under input limits with neural control barrier functions," in *Proceedings of (CoRL) Conference on Robot Learning*, December 2022, pp. 1–11.

[28] G. Schreiber, A. Stemmer, and R. Bischoff, "The fast research interface for the kuka lightweight robot," in *IEEE workshop on innovative robot control architectures for demanding (Research) applications how to modify and enhance commercial controllers (ICRA 2010)*. Citeseer, 2010, pp. 15–21.

[29] T. G. Molnar and A. D. Ames, "Composing control barrier functions for complex safety specifications," *IEEE Control Systems Letters*, vol. 7, pp. 3615–3620, 2023.

[30] W. Xiao and C. Belta, "Control barrier functions for systems with high relative degree," in *2019 IEEE 58th conference on decision and control (CDC)*. IEEE, 2019, pp. 474–479.